Regional recruitment of rat diaphragmatic lymphatics in response to increased pleural or peritoneal fluid load

Andrea Moriondo[1], Annalisa Grimaldi[2], Laura Sciacca[1], Maria Luisa Guidali[2], Cristiana Marcozzi[1] and Daniela Negrini[1]

[1]*Dipartimento di Scienze Biomediche Sperimentali e Cliniche and* [2]*Dipartimento di Biologia Strutturale e Funzionale, Università degli Studi dell'Insubria 21100 Varese, Italy*

The specific role of the diaphragmatic tendinous and muscular tissues in sustaining lymph formation and propulsion in the diaphragm was studied in 24 anaesthetized spontaneously breathing supine rats. Three experimental protocols were used: (a) control; (b) peritoneal ascitis, induced through an intraperitoneal injection of 100 ml kg^{-1} of iso-oncotic saline; and (c) pleural effusion, induced through an intrapleural injection of 6.6 ml kg^{-1} saline solution. A group of animals ($n = 12$) was instrumented to measure the hydraulic transdiaphragmatic pressure gradient between the pleural and peritoneal cavities in the three protocols. In the other group ($n = 12$), the injected iso-oncotic saline was enriched with 2% fluorescent dextrans (molecular mass = 70 kDa); at 30 min from the injections these animals were suppressed and their diaphragm excised and processed for confocal microscopy analysis. In control conditions, in spite of a favourable peritoneal-to-pleural pressure gradient, the majority of the tracer absorbed into the diaphragmatic lymphatic system converges towards the deeper collecting lymphatic ducts. This suggests that diaphragmatic lymph formation mostly depends upon pressure gradients developing between the serosal cavities and the lymphatic vessel lumen. In addition, the tracer distributes to lymph vessels located in the muscular diaphragmatic tissue, suggesting that active muscle contraction, rather than passive tendon stretch, more efficiently enhances local diaphragmatic lymph flow. Vice versa, a prevailing recruitment of the lymphatics of the tendinous diaphragmatic regions was observed in peritoneal ascitis and pleural effusion, suggesting a functional adaptation of the diaphragmatic network to increased draining requirements.

(Resubmitted 1 December 2006; accepted 9 January 2007; first published online 11 January 2007)
Corresponding author D. Negrini: Dipartimento di Scienze Biomediche Sperimentali e Cliniche, Università degli Studi dell'Insubria, Via J.H. Dunant 5, 21100 Varese, Italy. Email: daniela.negrini@uninsubria.it

The mechanism through which the initial lymphatic system exploits its homeostatic function in controlling the volume and solute composition of the tissue interstitial fluid is complex and composite. It is mostly accepted (Schmid-Schöenbein, 1990; Aukland & Reed, 1993) that lymph formation at tissue level, and subsequent centripetal propulsion of the newly formed lymph, depends upon two distinct processes: a so-called 'extrinsic mechanism' consisting of cyclic compressions and relaxations of the smallest initial lymphatics, as a consequence of tissue movements or muscle contraction, and/or the periodic squeezing of the lymphatic lumen performed by the spontaneous contraction of smooth muscle cells in the vessel wall ('intrinsic mechanisms').

Although in general both mechanisms may potentially contribute to lymph formation and propulsion, their actual role in setting and modulating lymph formation may be very variable in relation to the functional features of the tissue, the anatomical arrangement of the lymphatic network in a specific tissue and, last but not least, the high variability of the lymphatic vasculature features and performance even within the same tissue (Bridenbaugh *et al.* 2003; Gashev *et al.* 2004). Hence, while the strength and frequency of contraction of the lymphatic smooth muscle cells is the most important determinant of lymph flow modulation in, for instance, the mesenteric lymphatics or in the thoracic duct (Zawieja *et al.* 1993; Bridenbaugh *et al.* 2003; Gashev *et al.* 2004; von der Weid & Zawieja, 2004), this may not be true for lymphatic vessels supplying the thoracic tissues, which are evidently exposed to

A. Moriondo and A. Grimaldi equally contributed to this research.

 DOI: 10.1113/jphysiol.2006.127126

complex tissue displacements associated with the cardiac and respiratory cycles. In spontaneous breathing, lymph formation and propulsion in the intercostal lymphatics mostly depends upon cycles of compression/expansion of the lymphatic vessel lumen caused by the active contraction of inspiratory muscle rather than by the simple volume displacement (Moriondo *et al.* 2005). Additional smaller contributions to development of lymphatic transmural pressure gradients may be provided by cardiogenic tissue oscillations (Negrini *et al.* 2004) and probably, but not yet directly documented for the intercostal lymphatics, by the spontaneous intrinsic contractility (Negrini *et al.* 1994; Negrini & Del Fabbro, 1999) of the lymphatic vessel wall.

While intercostal lymphatics, because of their peculiar anatomical location, may be studied during spontaneous breathing, the lymphatic network over the pleural diaphragmatic dome can be visualized only after wide opening of the chest wall (Negrini & Del Fabbro, 1999; Negrini *et al.* 2004), maintaining cardiovascular functions by passive mechanical ventilation. Such an experimental approach allows evaluation of the role of the cardiogenic component of the extrinsic mechanism in diaphragmatic lymph function, but of course, cannot provide any indication of the contribution of the respiratory component in diaphragmatic lymph formation and in its flow modulation. It is worth noting that lymphatic vessels supply both the central diaphragmatic tendon and the peripheral skeletal muscle (Negrini *et al.* 1991, 1992; Grimaldi *et al.* 2006), tissues that behave very differently in terms of module and distribution of mechanical tissue stresses developing throughout the whole respiratory cycle. Therefore, the aims of the present research were to assess: (a) whether the muscular or the tendinous portions of the diaphragmatic lymphatic network are homogenously involved in the drainage of the peritoneal and pleural fluids in control conditions; (b) how the regional diaphragmatic lymphatics adapt to increased fluid load into the serosal cavities.

The outcome of this study might shed a light on the role of respiratory activity in modulating the diaphragmatic lymph flow in normal conditions; in addition, it might offer a possible mechanism to explain the development of pleural or peritoneal effusions in diseases characterized by an altered respiratory pattern or an impaired diaphragmatic contraction.

Methods

General preparation

Adult male Wistar rats (Charles River Italy, Calco, Lecco) were housed and experiments were performed in accordance to the National and institutional ethical committee guidelines of the local ethical committee. Rats (mean body weight 345 ± 23 g, $n = 24$) were anaesthetized with an intraperitoneal injection of a mixture made of 75 mg kg^{-1} ketamine (Sigma Aldrich, Milan, Italy) and 0.5 mg kg^{-1} medetomidine (Domitor, Pfizer) to induce deep surgical anaesthesia. Successive intraperitoneal boluses of a half dose of anaesthetic mixture were given if further required. Once deeply anaesthetized, the animals were turned supine on a warmed (37°C) blanket; tracheotomized; and an intratracheal cannula was connected to a heated pneumotacograph (Hans Rudolph, Inc., USA, model 8420) equipped with a dedicated pneumotach amplifier (Hans Rudolph, Inc. model 1110A) to continuously record respiratory flow. The flow signal was then digitized with a National Instruments BNC-2090 A/D board (100 Hz sampling rate), integrated though a dedicated LabView software (National Instruments Corporation, USA) to obtain respiratory tidal volume, and both flow and volume signals were then displayed on a monitor screen.

Arterial and venous pressures were measured through PE60 plastic saline-filled catheters inserted in the right carotid artery and jugular vein, respectively, and connected to physiological pressure tranducers (Model P23XL, Gould Electronics).

Pleural and peritoneal hydraulic pressure

A set of experiments ($n = 12$) was performed to quantify the transdiaphragmatic pressure gradient existing between the pleural and peritoneal space in normal conditions, or in the case of increased fluid volume (and pressure) in the pleural or peritoneal space. To this aim, the hydraulic pressure in the pleural (P_{pl}) and in the peritoneal (P_{abd}) spaces were simultaneously measured through blunted saline-filled stainless steel cannulas (length: 5 cm; external diameter: 0.5 mm; internal diameter: 0.3 mm) connected to pressure transducers (Gould Electronics, model P23XL) and inserted in the supradiaphragmatic and subdiaphragmatic regions, respectively, according to a previously described procedure (Miserocchi *et al.* 1982). At the insertion side, the tip of the cannula was perforated with 3–4 tiny lateral holes. With the animals lying supine, the skin and superficial tissues on the right side of the thorax and on the upper abdomen were removed. The pleural cannula was inserted in the 7–9th intercostal space by gently pushing through the internal intercostal muscles to position the cannula tip medially over the diaphragmatic dome. The insertion was performed under a flush of saline to avoid air entrance into the pleural space. Subsequently, the peritoneal cannula was inserted through the lateral wall of the abdomen and it was driven along the cranial surface of the liver to position the cannula tip in the subdiaphragmatic medial region. The cannulae were placed horizontally at the same height, within 1 cm of

the bottom part of the pleural and peritoneal space. To facilitate the allocation of the cannulae in the supra- and subdiaphragmatic regions, the cannulae were shaped to adapt to the diaphragmatic dome curvature. The exact location of the recording cannula tip was assessed on opening the pleural and peritoneal cavity at the end of the experiment.

Systemic arterial and venous, pleural and peritoneal hydraulic pressures were monitored from the baseline condition to the end of the experiments, at 180 min from the pleural or peritoneal injections, by conveying the signal output from the pressure transducers to the corresponding amplifiers in a signal conditioner (Model 6600, Gould Electronics).

For the pleural and peritoneal pressure measurements, three groups of rats were used: (a) control ($n = 6$). In the rats belonging to this group, P_{pl} and P_{abd} were measured under baseline conditions and for 180 min after either the injection of 0.2 ml of saline solution containing 2 g dl^{-1} of serum albumin (Sigma Aldrich, Milan, Italy) in the pleural space ($n = 3$), or after the injection of 1 ml of the same solution into the peritoneal space ($n = 3$); (b) peritoneal ascitis ($n = 3$). After insertion of the recording cannulae in the pleural and peritoneal cavities, experimental ascitis was induced by injecting into the peritoneal cavity 100 ml kg^{-1} of 2 g dl^{-1} albumin solution through the intraperitoneal cannula. No fluid was added to the pleural space; (c) pleural effusion ($n = 3$). In this group, experimental pleural effusion was induced by injection 6.6 ml kg^{-1} of saline solution containing 2 g dl^{-1} of serum albumin (Sigma Aldrich, Milan, Italy) into the pleural space through the intrapleural cannula. No injection was given in the peritoneal space. In groups b and c, pleural and peritoneal fluid pressure were measured before and up to 180 min from the pleural or peritoneal injection, for a total of about 200 min, after which the animals were suppressed with an anaesthesia overdose.

The net transdiaphragmatic hydraulic pressure gradient (ΔP_{TD}) developing between the pleural and the peritoneal cavities was calculated as $\Delta P_{TD} = P_{pl} - P_{abd}$.

Imaging of a fluorescent tracer distribution in the diaphragm

In a parallel series of experiments ($n = 12$), we investigated the effect of the transdiaphragmatic pressure gradients on the exchange of large solutes between the pleural and peritoneal cavities through the diaphragmatic lymphatics. To this aim, high-molecular weight fluorescent dextrans were injected into the pleural or peritoneal cavity according to the following protocol: (d) control ($n = 6$). After the general preparation, 0.2 ml of physiological saline solution containing 70 KDa FITC-conjugated dextrans (2% in saline; Sigma Aldrich, Milan, Italy) or 1 ml of 70 KDa Rodamine (TRITC)-conjugated dextrans (2% in saline; Sigma Aldrich, Milan, Italy) were injected into the pleural ($n = 3$) or peritoneal ($n = 3$) space. Injections were performed through blunted hypodermic needles that were removed immediately after the injections. P_{pl} and P_{abd} were not measured in these experiments; (e) peritoneal ascitis ($n = 3$). Experimental ascitis was induced by injecting 100 ml kg^{-1} of Rodamine (TRITC)-conjugated dextrans in the peritoneal cavity, with no tracer in the pleural space; (f) pleural effusion ($n = 3$). This group received 6.6 ml kg^{-1} of FITC-conjugated dextrans in the pleural cavity and no dextrans in the peritoneal cavity. Animals were suppressed with an anaesthesia overdose at 30 min after dextran injection. At the end of the experiments, the whole diaphragm was immediately excised and cut into eight large pieces of approximately the same size, belonging to four distinct diaphragmatic regions, as depicted in Fig. 1: (a) a ventrolateral portion (region 1), corresponding to the peripheral muscular area of the ventral diaphragm; (b) a medial ventral portion (region 2), corresponding to the tendinous area of the ventral diaphragm; (c) a dorsolateral muscular region (region 3); and (d) a dorsal medial tendineous region (region 4).

The diaphragmatic tissue belonging to each of the four regions was dissected into small pieces and prepared for subsequent morphological analysis.

Experiments of groups a and d (controls), b and e (ascitis) and c and f (pleural effusion) were conducted in pairs: one rat received the fluorescent dextran injection, a second rat of same weight (±5% weight difference) was injected with 2% BSA-saline only, and was used for the measurement of physiological parameters during

Figure 1. Sketch of the frontal view of the diaphragm
The shaded areas correspond to the medial tendinous tissue (light shading) and the peripheral skeletal muscle (dark shading). The dashed superimposed lines identify four regions into which both the pleural and peritoneal diaphragmatic surfaces have been divided to proceed with the tracer distribution analysis: region 1, ventrolateral area corresponding to ventral peripheral muscular portion; region 2, medial ventral portion corresponding to ventral tendineous area; region 3, dorsolateral muscular region; region 4, dorsomedial tendinous region.

the whole experiment time. The rats used for P_{pl} and P_{abd} recordings were not utilized for the analysis of tracer invasion into the diaphragmatic lymphatics because the pressure-recording cannulae might have somehow damaged or scratched the diaphragmatic surface, thus affecting the result of the morphological analysis.

Confocal microscopy

In order to perform a quantitative analysis of the tracer distribution in the diaphragmatic lymphatics, small blocks (~5 mm side) excised from the diaphragmatic regions 1–4 were immediately embedded in polyfreeze cryostat embedding medium (OCT, Polyscience Europe, Eppelheim, Germany) and frozen in liquid nitrogen. Cryosections of diaphragm (10 μm thick) were obtained with a Reichert Jung Frigocut 2800. Slides were mounted in Vectashield mounting medium for fluorescence (Vector Laboratories, Burlingame, California), and examined with a confocal laser microscope Olympus (laser λ 488 nm for FITC and laser λ 568 nm for TRITC).

Image analysis of fluorescence invasion

Quantitative analysis of dextran distribution was performed on digitally acquired fluorescence images by SimplePCI software (Compix Inc., Sewickley, PA USA). In order to quantify the distance travelled by the fluorescent dextrans within the diaphragm, images of the whole diaphragm transverse sections were processed as follows. The fluorescent spots, representing FITC- or TRITC-filled lymphatic vessels, were quantified by binary conversion of the fluorescent signal; the surface area of each spot was expressed in absolute numbers, and the sum of all fluorescent areas detected by the image-acquisition system was set equal to 100%. To cope with the variability of the diaphragmatic thickness between different animals and within the investigated region, the label invasion into the lymphatic network was expressed as the cumulative percentage labelling, plotted as a function of the fractional distance from the side of injection (0%) to the opposite side (100%).

For each of the four diaphragmatic regions three diaphragmatic specimens, one from each rat, were analysed and the cumulative percentage invasions of the label in the three specimens were pooled and shown in the same plot, which was then representative of the tracer behaviour in the three animals belonging to the same group.

Data analysis

Data are reported as mean ± 1 S.D. Absolute values were compared by one-way ANOVA. Differences between mean values were considered significant at $P < 0.05$. Whenever one-way ANOVA detected a significant difference between mean values, all pairwise multiple comparison procedures were performed (Bonferroni t test).

Results

An example of the rat intraperitoneal (P_{abd}) and intrapleural (P_{pl}) pressure recordings is presented in Fig. 2, which shows the tidal volume (V_T), and the P_{abd} and P_{pl} traces during spontaneous breathing before tracer injection and after induction of experimental peritoneal ascitis (Fig. 2*B*) or pleural effusion (Fig. 2*A*). Pre-injection P_{pl} and P_{abd} over the entire respiratory cycle averaged -0.31 ± 0.06 mmHg (range -0.26 to -0.66 mmHg, $n = 9$), and 0.02 ± 0.16 mmHg (range -0.26 to 0.85 mmHg, $n = 9$), respectively. The average transdiaphragmatic pressure gradient $\Delta P_{TD} = P_{pl} - P_{abd}$ was -0.33 ± 0.4 mmHg (range -1.11 to -0.22 mmHg), the negative sign indicating a peritoneal-to-pleural ΔP_{TD}.

The inspiratory-to-expiratory time ratio calculated from the V_T curves was 0.22 ± 0.04 (range 0.18 to 0.25) in control, 0.20 ± 0.06 (range 0.13 to 0.23) in ascitis and 0.28 ± 0.07 (range 0.23 to 0.36) in experimental pleural effusion. Neither of the latter two values was significantly different from control, albeit a significant ($P < 0.05$) increase of the respiratory rate was observed in pleural effusion (48.8 ± 4.6 cycles min^{-1}; range 41.1 to 59.4 cycles min^{-1}) compared to control (25.9 ± 1.1 cycles min^{-1}; range 19.2 to 27.5 cycles min^{-1}) due to a shorter expiratory pause.

In control rats (group a), which received the injection of 0.2 ml in the pleural cavity, P_{pl} increased by 1.03 ± 0.05 mmHg (range 0.95 to 1.19 mmHg) immediately after the injection and thereafter returned to baseline values within 483 ± 35 s (range 436 to 516 s) from the beginning of the injection phase. In control rats receiving 1 ml in the peritoneal cavity, P_{abd} remained essentially unchanged with respect to baseline values. In these control experiments, the local transient pressure change induced by the injection in one cavity was not significantly transmitted across the diaphragm to the other serous space, whose hydraulic pressure remained essentially unchanged during the injection manoeuvre.

In experimental ascitis (group b), P_{abd} significantly increased from a pre-injection value of $+0.15 \pm 0.2$ mmHg (range -0.89 to 0.35 mmHg), to 1.82 ± 0.10 mmHg (range 1.70 to 1.93 mmHg, $P < 0.05$, $n = 3$) upon saline-BSA injection and remained substantially stable for the following 180 min (Fig. 3*A*). Although P_{pl} was essentially unaffected by the intraperitoneal injection, the transdiaphragmatic ΔP_{TD} became significantly more subatmospheric (-2.28 ± 0.31 mmHg, range -2.59 to -1.98 mmHg, $P < 0.05$, $n = 3$) compared to the pre-injection value (-0.62 ± 0.03 mmHg, range -0.88 to -0.39 mmHg).

In the pleural effusion (group c), P_{pl} significantly increased from a control value of -0.55 ± 0.07 mmHg (range -0.63 to -0.48 mmHg) to 0.61 ± 0.01 mmHg (range 0.48 to 0.81 mmHg, $P < 0.05$, $n = 3$), whereas P_{abd} remained unchanged upon intrapleural injection of saline-BSA. As a results, ΔP_{TD} increased from -0.31 ± 0.13 mmHg (range -0.41 to -0.22 mmHg) at pre-injection baseline to 0.88 ± 0.11 mmHg upon injection (range 0.09 to 1.32 mmHg, $P < 0.05$, $n = 3$). At variance with what was observed in experimental ascitis (Fig. 3*A*), the increase in P_{pl} and thus in ΔP_{TD} was transient (Fig. 3*B*), and after 30 min from the injection both parameters had already returned to values not significantly different from the control, pre-injection ones (Fig. 3*B*).

Tracer distribution with normal peritoneal and pleural fluid volume

Typical cross-sectional images of the diaphragm after injection of the fluorescent tracer into one of the cavities are presented in Fig. 4*A–D*, where the red and green fluorescent spots identify the distribution of TRITC (red spots) or FITC (green spots) injected in the peritoneal or pleural cavity, respectively.

The cumulative percentage invasion of the TRITC-conjugated dextrans injected in the peritoneal space under control condition (group d) is illustrated in Fig. 5*A*; the zero on the *x* axis represents the site of injection, i.e. in this instance, the peritoneal surface of the diaphragm, while 100% corresponds to the opposite diaphragmatic surface, i.e. in this case, the pleural side. The slope of the proposed relationship is an index of the amount of label accumulated at 30 min at a given depth within the diaphragm with respect to the lymphatic entrance at the diaphragmatic surface.

Figure 5*A* encompasses data from all muscular and tendinous regions, and indicates that at 30 min after the peritoneal injection, the fluorescence signal can be found almost completely in the peritoneal half-side of the diaphragmatic lymphatic network. An attempt is made in Table 1 to correlate the fractional depth reached by

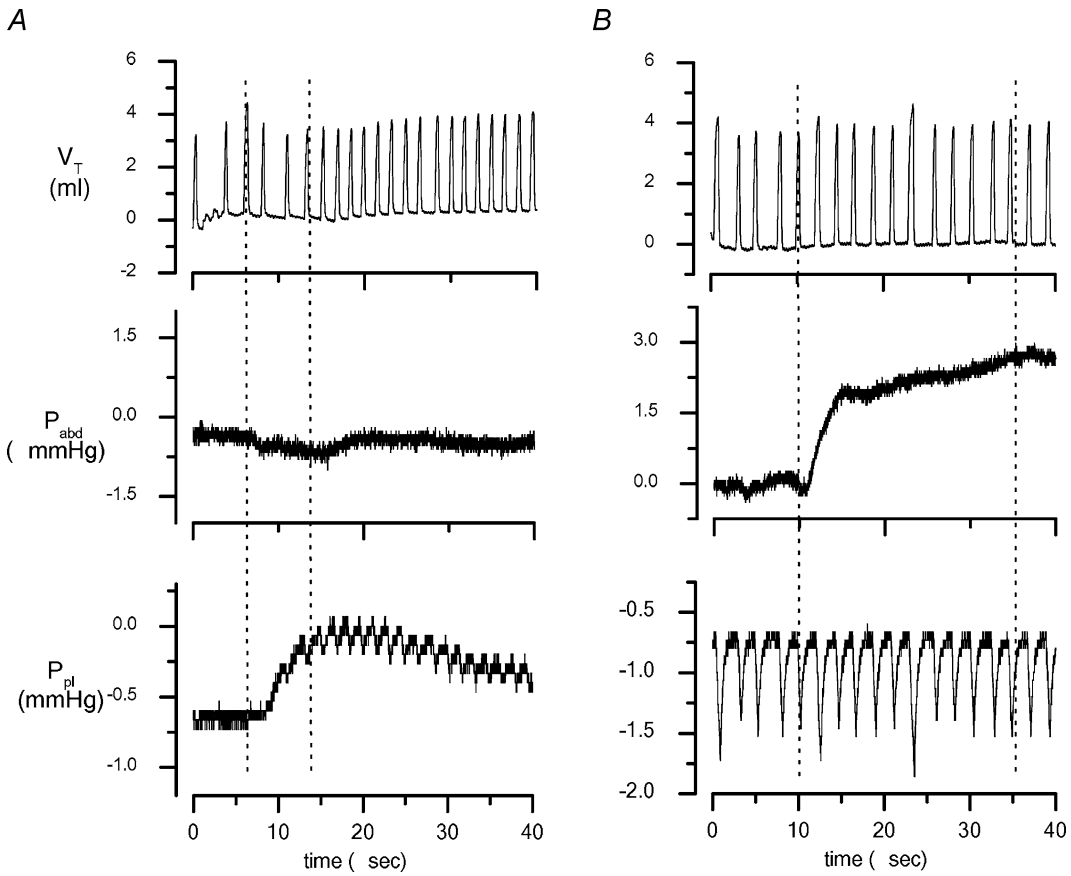

Figure 2. Example of traces of tidal volume (V_T), subphrenic abdominal pressure (P_{abd}) and supraphrenic pleural pressure (P_{pl}) recorded in baseline conditions and after induction of experimental pleural effusion (*A*) and peritoneal ascitis (*B*)

The vertical dashed lines delimit the time interval needed to complete the infusion procedure and it was much longer in the case of the much larger injection in the peritoneal cavity.

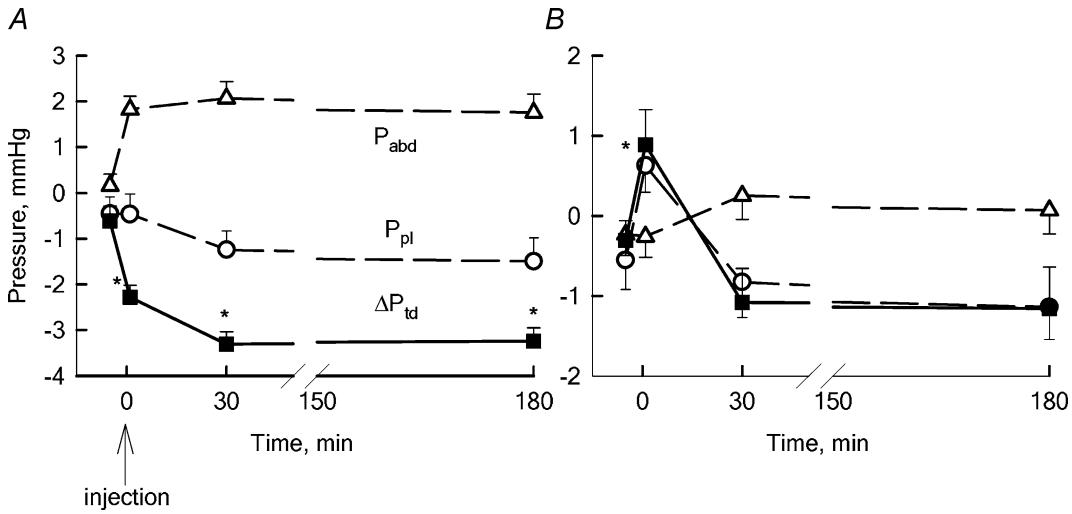

Figure 3. Average P_{abd} (△) and P_{pl} (○) values in control pre-injection baseline and after tracer injection into the peritoneal (*A*) and pleural (*B*) cavities
The transdiaphragmatic hydraulic pressure gradient (ΔP_{TD}, ■) was calculated as: $\Delta P_{TD} = P_{pl} - P_{abd}$. Injection was performed at time = 0. A negative ΔP_{TD} signifies a potential fluid flow from the peritoneal to the pleural space. In experimental ascitis, the peritoneal-to-pleural ΔP_{TD} further increased with respect to the pre-injection baseline value, remaining stable up to 180 min after intraperitoneal injection. On the other hand, pleural effusion reversed the pre-injection ΔP_{TD} value causing the development of a transient pleural-to-peritoneal ΔP_{TD} that was completely nullified at 30 min from injection (*B*). *Significantly different ($P < 0.05$) from pre-injection baseline values.

the label within the diaphragmatic thickness with the actual morphology of the lymphatic three-dimensional arrangement. Based on a recent morphological description of the different structures belonging to the diaphragmatic lymphatic network and on their average depth within the diaphragmatic thickness (Grimaldi *et al.* 2006), it is possible to locate the fluorescent labels in the pleural and peritoneal submesothelial lacunae, in the trans-

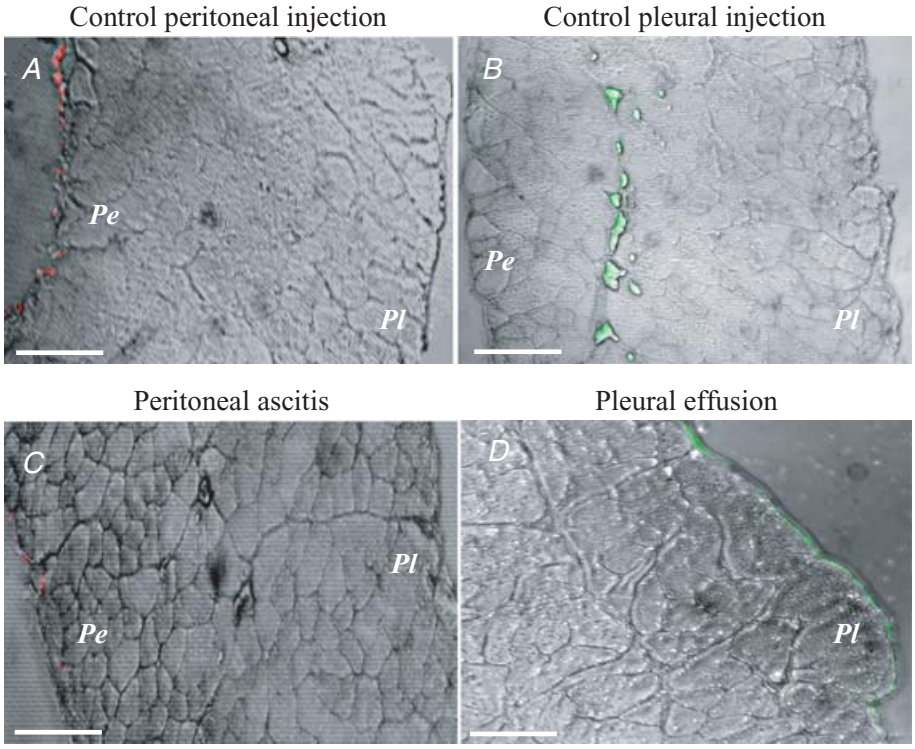

Figure 4. Confocal microscope cross-section images of the diaphragm after injection of TRITC (red spots) or FITC (green spots) in the peritoneal or pleural cavity, respectively
Pe, peritoneal side; Pl, pleural side. *A–C*, scale bars correspond to 150 μm; *D*, bar corresponds to 100 μm.

verse ducts of the pleural or peritoneal side of the diaphragm, or in the larger collecting lymphatics running in the deeper diaphragmatic tissue. In control peritoneal injection (Fig. 5*A*), ~85% of the label was localized in the transverse peritoneal ducts (Table 1, column 3), with the remaining 15% in the central collectors representing the outflow lymphatics. Only negligible fractions (<1%) were found towards the pleural side. A distinction between the location of the label in the tendinous and in the muscular portions is proposed in Fig. 5*B*, where the cumulative label distribution within a given region is shown, expressed as a percentage of the regional label count. About 90% of the label distributed in the tendinous region (○) is confined in the 20% of the diaphragm thickness proximal to the peritoneal side, while a deeper invasion of the label is observed in the muscular regions (●).

When fluorescent dextrans were injected in the pleural space (Fig. 6*A*), they rapidly entered the initial lymphatic system, as indicated by the observation that, at 30 min, ~90% of the label was found deep in the diaphragm, corresponding with the pleural transverse and collecting ducts (Table 1, column 4). Unlike what was observed with peritoneal control injection (Fig. 5*A*), the fluorescent dye crossed the entire diaphragm reaching the peritoneal side. In addition, label invasion was faster in the lymphatics of the muscular than the tendinous regions, a phenomenon similar to, although more evident than, that observed with the control peritoneal injection (Fig. 5*B*).

Tracer distribution in experimental acute peritoneal ascitis

At 30 min from the induction of experimental ascitis (Fig. 7*A*, asterisks), the fluorescent dye was more homogeneously distributed within the diaphragmatic thickness compared to what was observed in control peritoneal injection (◇, from Fig. 5*A*), invading not only the peritoneal transverse and central collecting ducts, but spreading into the pleural transverse vessels as well (Table 1, column 5). While the label distribution in the muscular portion was essentially unchanged with respect to control peritoneal injection (Fig. 5*B*), the dextran invasion into the tendineous lymphatics was scattered, resulting in the irregular shape of the total distribution plot in Fig. 7*A*. Hence, we further analysed the percentage label distribution in the tendinous area, by differentiating between the ventral and the dorsal tendinous regions (areas 2 and 4 in the sketch of Fig. 1), whose percentage distribution is presented in Fig. 7*B* and *C* (△) and compared to the distribution obtained for the same regions after the control peritoneal injection (Fig. 7*B* and *C*, ○). Data indicate that, while the experimental condition (control peritoneal injection or ascitis) had only a minor effect on the label distribution in the ventral tendinous region (Fig. 7*B*), it substantially modified the fluorescent invasion in the dorsal tendineous one (Fig 7*C*), facilitating the label invasion towards the opposite pleural diaphragmatic surface in comparison with control. These

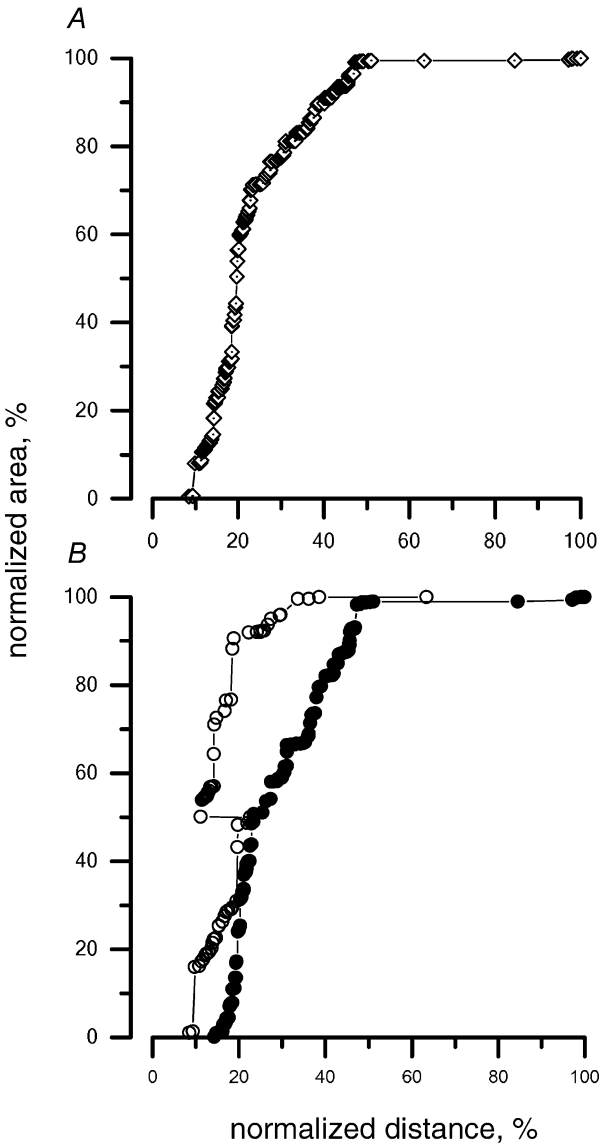

Figure 5. Cumulative percentage distribution of the tracer injected into the peritoneal cavity under control condition within the diaphragmatic lymphatic network after 30 min from the injection

A, the area of the fluorescent spots visualized in the confocal microscope images (see the example in Fig. 4), normalized as a percentage of the area of all fluorescent spots from the muscular and tendinous regions, is presented as a function of the distance from the diaphragmatic surface at the side of injection. On the *x* axis, the distance travelled by the fluorescent tracer within the diaphragm was normalized, indicating 0% as the diaphragmatic surface facing the injection site and 100% as the whole diaphragmatic thickness. Hence, in cases where the tracer was injected into the peritoneal cavity, 0% and 100% on the *x*-axis correspond to the peritoneal and pleural diaphragmatic surfaces, respectively. *B*, cumulative percentage distribution of the tracer in the tendinous (○) and muscular (●) regions.

Table 1. Percentage distribution of the fluorescent dextrans attained in the various experimental conditions

		Control (%)		Volume load (%)	
% Distance from pleural surface	Lymphatic structure	Peritoneal injection	Pleural injection	Peritoneal ascitis	Pleural effusion
0–4	Pleural submesothelial lacunae (∼33 μm)	0.35	0.77	0.17	1.98
4–37	Pleural transverse ducts (∼245 μm)	0.19	39.62	21.92	47.35
37–64	Central collectors (∼200 μm)	15.52	50.96	22.09	38.84
64–97	Peritoneal transverse ducts (∼245 μm)	83.94	8.65	55.82	11.83
97–100	Peritoneal submesothelial lacunae (∼19 μm)	0	0	0	0

Percentage distribution of the fluorescent dextrans attained in the various experimental conditions (control peritoneal injection, column 3; control pleural injection, column 4; ascitis, column 5; pleural effusion, column 6) in the different segments of the diaphragmatic lymphatics (as described by Grimaldi *et al.* 2006): submesothelial pleural lacunae, transverse ducts originating from the pleural lacunae, central collectors, transverse ducts originating from the peritoneal lacunae and submesothelial pleural lacunae. The percentage (column 1) and absolute (column 2) diaphragmatic thickness corresponding to the location of the above structures are from Grimaldi *et al.* (2006), for an average diaphragmatic thickness of 743 μm. In column 1, the distance from the pleural surface is expressed as percentage of the total diaphragmatic thickness, where 0% and 100% represents the pleural and peritoneal surface, respectively.

data suggest that, when challenged with expanded volume load, a differential gravity-dependent recruitment of the tendinous diaphragmatic lymphatics may occur.

Tracer distribution in experimental acute pleural effusion

The cumulative label distribution at 30 min after induction of experimental pleural effusion (Fig. 8*A*, asterisks and Table 1, column 6) was not significantly modified compared to the control pleural injection (Fig. 8*A*, ◇). However, unlike what was observed with ascitis, the lymphatic invasion of the label in the muscular region (Fig. 8*B*, ■) was definitely modified with respect to control (Fig. 8*B*, ●), most of the tracers remaining confined in the pleural portion of the diaphragm. On the other hand, the tendinous regions (Fig. 8*C*, □) displayed an opposite behaviour, being subject to an easier invasion of the label with respect to control pleural injection (Fig. 8*C*, ○). No gravity-dependent difference was observed in either the tendinous or muscular regional distribution of the label.

Discussion

The diaphragmatic lymphatic network is organized in a series of confluent ducts originating from the stomas, porous-like direct openings located at the rims of adjacent mesothelial cells opening directly over the pleural and peritoneal cavities within the corresponding mesothelial layers (Wang, 1975; Ohtani *et al.* 1993; Grimaldi *et al.* 2006). Because of their diameter (from less than 1 μm to 20–30 μm (Wang, 1975; Negrini *et al.* 1991), solutes of molecular weight as large as cells may easily enter the stomas to subsequently converge into the deeper submesothelial lymphatic structures (Negrini *et al.* 1992; Grimaldi *et al.* 2006). On the contrary, adjacent mesothelial cells are connected through intercellular tight junctions and desmosomes (Mariassy & Wheeldon, 1983; Wang, 1998) that limit paracellular transport of large solutes to the submesothelial interstitium. In the normal rat diaphragm, collagen bundles connect the outer surface of the vascular and lymphatic endothelium to the tissue and skeletal muscle fibres, creating a selective tight interstitial fibre mesh (Grimaldi *et al.* 2006), through which diffusion of large particulate matter may be hindered. Within the diaphragm, transit of fluid and solutes drained from the pleural and peritoneal spaces is expected to occur mostly through lymphatic vessels, which provide a much lower-resistance pathway with respect to viscous flows. Therefore, the dextran distribution observed in our study probably reflects a lymphatic transit rather than a diffuse interstitial spreading of the tracer.

Control injections caused only minor and transient ($<$40 s) increase in P_{pl}, and no changes in P_{abd}, so that the ΔP_{TD} was essentially unaffected; therefore, the path followed by dextrans in these conditions may actually mirror the normal distribution of large-molecular weight molecules into the diaphragmatic lymphatics.

The increased peritoneal or pleural fluid loads were used in order to study the effect of a ΔP_{TD} change on the diaphragmatic tracer distribution. No signs of local or systemic inflammation developed in our acute short-term experiments, in which, unlike what observed in clinical stages of pleural effusion or ascitis (Michailova, 2001), the permeability of the pleural and peritoneal mesothelia and of the lymphatic endothelium are presumably still normal. Therefore, we believe the present experimental approach is best suited for following dextran progression into the diaphragmatic lymphatics down an imposed pressure gradient.

Although we extended the P_{abd} and P_{pl} measurements up to 3 h from dextran injection, we limited the confocal microscopy analysis to the first 30 min. Dextrans removed from the cavities into the diaphragmatic lymphatics may actually recirculate through the blood back into either the pleural or peritoneal space, to be subsequently re-absorbed into the lymphatic system, thus interfering with the original dextran distribution. Limiting the image observation at 30 min from injection thus allowed us to focus on the early distribution of dextrans within the diaphragmatic lymphatic regions.

The present experimental approach would not have been adequate to quantify the transdiaphragmatic transfer of dextrans between the pleural and peritoneal space, an investigation that would require an accurate mass balance analysis (Lai-Fook *et al.* 2005) that is beyond the targets of the present study.

Tracer distribution into diaphragmatic lymphatics

One of the main indications of the present results is that the diaphragmatic lymphatics behave like a diffuse intradiaphragmatic network to optimize the lymphatic drainage of the pleural and peritoneal cavities, meanwhile assuring an almost complete separation between the two serous cavities. Indeed, in control, more than 90% of the tracer accumulated in the transverse ducts proximal to the dextran injection site and in the deeper central collectors (Figs 5 and 6, Table 1). With increasing serosal fluid accumulation, a sequential recruitment of the whole lymphatic network was observed (Figs 7 and 8, respectively). However, even in this condition, at 30 min from the injection, the majority of the tracer was still localized in the transverse lymphatic ducts proximal to the site of injection and in the deeper central collectors (see Table 1), while less than 1% of the tracer, if any, stained the submesothelial lacunae opposite to the site of injection.

Under physiological steady state, P_{abd} was only slightly higher than P_{pl} during the whole respiratory cycle (see Results and Fig. 3*A* and *B*), so that a net peritoneal-to-pleural ΔP_{TD} barely developed. In line with this observation, no significant transfer (<0.5%) of high-molecular weight dextrans was observed in the control condition from the peritoneal to the pleural side, the greatest majority of the tracer being localized in the peritoneal transverse ducts (84%, Table 1 and Fig. 5) or in the deeper central collectors.

The increased ΔP_{TD} at the onset of experimental ascitis (Fig. 3*A*) favoured a more homogenous spreading of the tracer within the lymphatic network, but did not substantially modify its transfer to the subpleural diaphragmatic lymphatics, as indicated by the fact that only 0.17% of the tracer was found in the pleural submesothelial lacunae (Table 1). Similarly, a favourable pleural-to-peritoneal ΔP_{TD} at the onset of experimental pleural effusion (Fig. 3*B*) caused a more homogenous distribution of dextrans into the deeper lymphatics, but not in the peritoneal submesothelial ones (Table 1).

Based on this evidence, progression of tracer within the diaphragmatic lymphatic network seems to depend

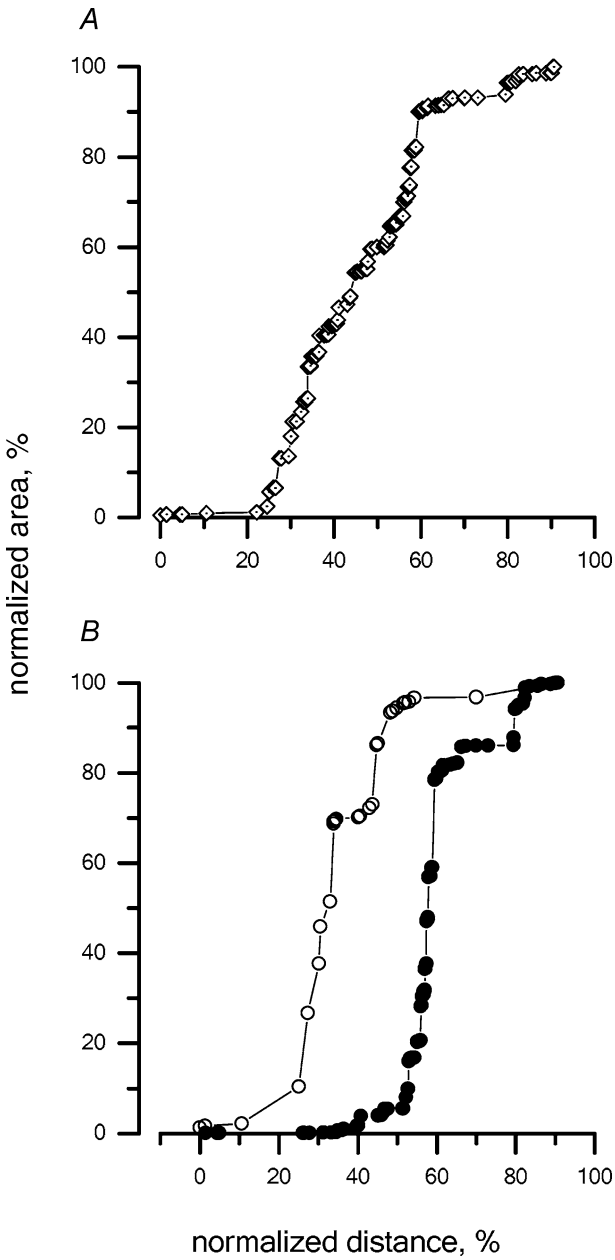

Figure 6. Cumulative percentage distribution of the tracer injected into the pleural cavity under control conditions within the diaphragmatic lymphatic network at 30 min from the injection

In this case, since the tracer was injected into the pleural space, 0 and 100% on the *x* axis correspond to the pleural and peritoneal diaphragmatic surfaces, respectively. *A*, cumulative percentage distribution of the tracer in the diaphragmatic lymphatics, including all muscular and tendinous regions. *B*, cumulative percentage distribution of the tracer in the tendineous (○) and muscular (●) regions.

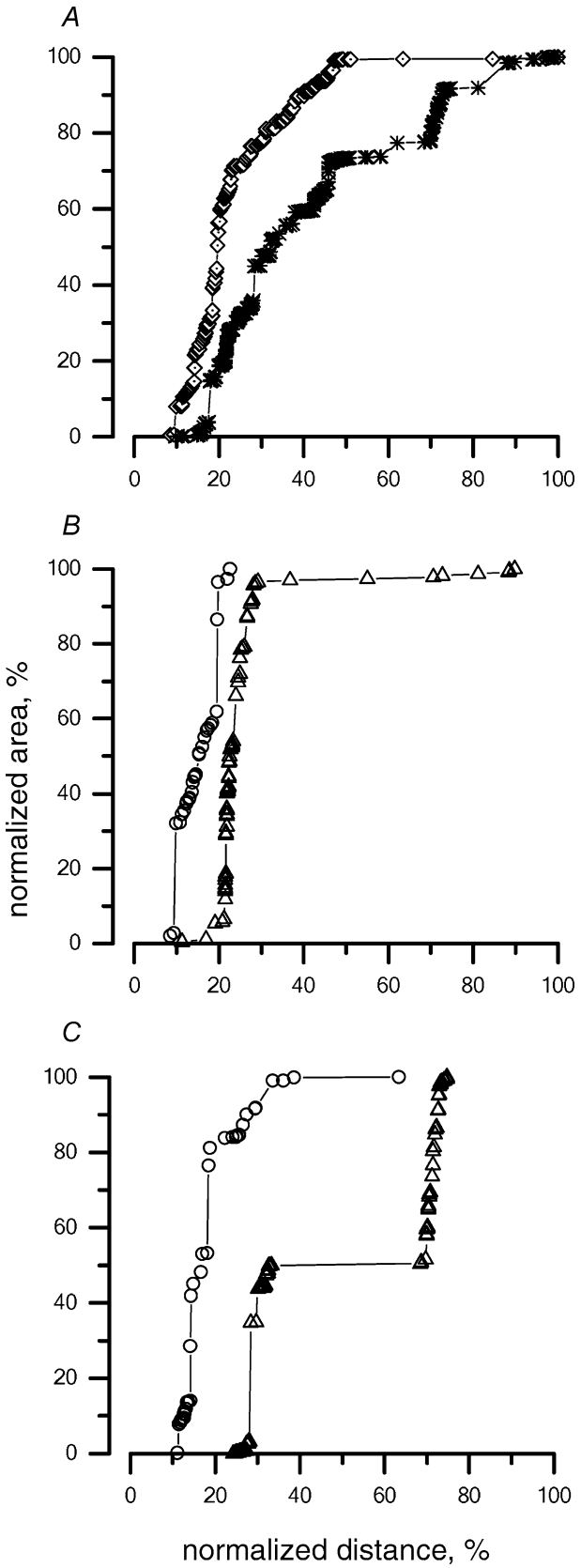

not upon ΔP_{TD}, but rather upon the pressure gradients developing between the pleural or peritoneal cavities and the lumen of the diaphragmatic lymphatic vessels. Direct micropuncture measurements have revealed that the hydraulic pressure in the lumen of the diaphragmatic submesothelial lymph vessels (P_{lymph}) is as low as −10 mmHg (Negrini & Del Fabbro, 1999; Negrini *et al.* 2004; Grimaldi *et al.* 2006), i.e. much lower than the end-expiratory P_{pe} recorded at the same height in the diaphragmatic pleural space (Miserocchi *et al.* 1982; 1984; Negrini *et al.* 1993). A similar situation probably holds for the peritoneal diaphragmatic lymphatics, whose absorbing pressure in spontaneously breathing rabbits is of the order of ∼−5 mmHg (Miserocchi *et al.* 1989). Hence, the net driving pressure gradient developing between the pleural or peritoneal cavities and the lumen of diaphragmatic lymphatics significantly outranks ΔP_{TD}. This might explain the confluence of the tracer, irrespective of the injection site, towards the deeper collecting duct, as well as the efficiency of the labelled dextrans removal from the pleural diaphragmatic area in the face of an adverse ΔP_{TD}.

The relative absence of tracer in the submesothelial lacunae might simply reflect their small volume capacity; in fact, the thickness of the whole submesothelial interstitial space, in which the lacunae lay, only occupies ∼5–6% (∼20–30 μm) of the total diaphragmatic tissue thickness (Table 1; Grimaldi *et al.* 2006). On the other hand, the relative emptiness of the submesothelial lacunae may also reflect a fast removal of the tracer towards the deeper ducts which represent the final egress route for diaphragmatic lymph. The fast transfer of tracers and fluid might, in turn, be facilitated by the pressure distribution within the lymphatic network and by the two unidirectional valve system recently described in the diaphragmatic lymphatics (Grimaldi *et al.* 2006). From this standpoint one might observe that, in control

Figure 7. Distribution of the tracers in the diaphragmatic lymphatics at 30 min after induction of experimental ascitis, as a function of the normalized diaphragmatic thickness
The 0% and 100% on the *x*-axis correspond to the peritoneal and pleural diaphragmatic surfaces, respectively, *A*, cumulative percentage distribution of the tracer in all muscular and tendinous regions at 30 min from induction of ascitis (*) with respect to control peritoneal injection (◇, from Fig. 5*A*). *B*, cumulative percentage distribution of the tracer in the tendineous ventral region (region 2 in Fig. 1) at 30 min from induction of ascitis (△) with respect to control peritoneal injection (○). Apart from a small invasion of the label towards the opposite pleural surface of the diaphragm, no major difference compared to control was observed. *C*, cumulative percentage distribution of the tracer in the tendinous dorsal region (region 4 in Fig. 1) at 30 min from induction of ascitis (△) with respect to control peritoneal injection (○). The modification of the tracer distribution within the diaphragmatic lymphatics suggests a higher recruitment of the tendinous lymphatic pathways in ascitis compared to control.

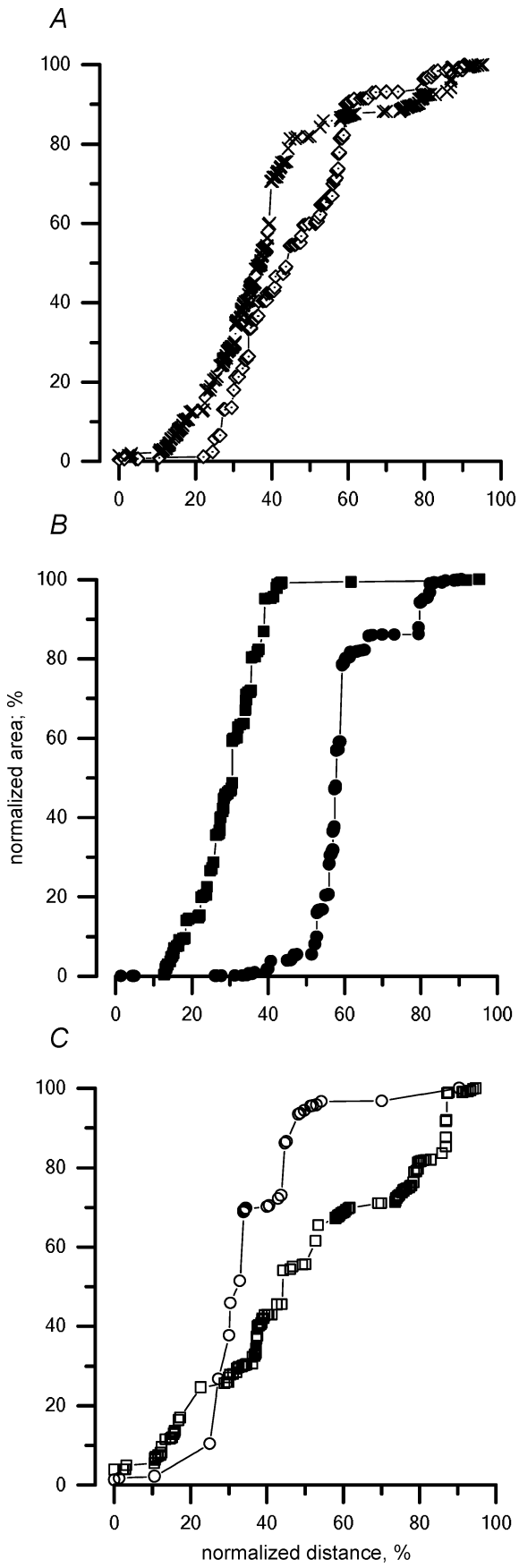

conditions, at 30 min from the pleural injection, only about 40% of the tracer is still localized in the pleural submesothelial lacunae and transverse ducts (Table 1), the majority of the tracer having already discharged into the deeper collectors. Conversely, in control peritoneal injection, notwithstanding the persistence of a positive P_{abd}, almost 85% of the tracer is still contained in the peritoneal transverse ducts, with only ∼15% in the deep central collectors (Table 1). This difference might reflect a higher draining efficiency of the pleural compared to the peritoneal diaphragmatic lymphatics, and might be functional to the maintenance of a 'dry' pleural cavity, at least under physiological steady state.

Contribution of muscular and tendineous diaphragmatic lymphatics in control conditions

The present data suggest a different involvement of the lymphatics located in the skeletal muscle compared to those in the central tendon. In fact, in control (Figs 5*B* and 6*B*) the cumulative tracer distribution in lymphatics of muscular regions 1 and 3 (Fig. 1) is shifted to the right compared to the tendineous regions 2 and 4, suggesting a more efficient tracer entrance in lymphatics of the muscular regions in the face of the higher density of stomata and lacunae observed in tendinous regions (Negrini *et al.* 1991; 1992). In spontaneous breathing at end expiration, the peripheral skeletal muscle fibres (see sketch in Fig. 1) are relaxed at their resting tone and length, while the radial stretch applied to the medial tendinous fibres is released. On the other hand, on inspiration, as the muscle fibres contract and shorten inward, the tendineous ones are pulled outward. Interstitial pressure (P_{int}) in the diaphragmatic muscle and tendon have never been

Figure 8. Distribution of the tracers in the diaphragmatic lymphatics at 30 min after induction of experimental pleural effusion
Since tracer was injected into the pleural space, 0% and 100% on the *x* axis correspond to the pleural and peritoneal diaphragmatic surfaces, respectively. *A*, cumulative percentage distribution of the tracer in all regions at 30 min from induction of pleural effusion (*) with respect to control (◇). No substantial differences in tracer distribution were found between the two conditions. *B*, cumulative percentage distribution of the tracer in the muscular regions (regions 1 and 3 in Fig. 1) after pleural effusion (■) with respect to control (●). In face of the similarity between the overall tracer distribution in the two experimental conditions (Fig. 8*A*), the cumulative relationship was clearly shifted to the left after pleural effusion, suggesting a decreased involvement of the deeper lymphatic vessels belonging to the muscular regions in lymphatic removal of the pleural cavity in pleural effusion. *C*, cumulative percentage distribution of the tracer in the tendineous regions (regions 2 and 4 in Fig. 1) at 30 min after pleural effusion (□) with respect to control (○). A shift to the right of the tracer distribution pattern suggests a more homogeneous involvement of all sections of the tendinous portion of the diaphragmatic lymphatic net after pleural effusion with respect to control.

measured during spontaneous breathing, but one would expect P_{int} to increase in the muscle during inspiration when the muscle contracts and shortens, compressing the lymphatic vessel lumen and opposing lymph progression in the muscular lymphatics. In normal breathing, a long expiratory pause (∼70% of the respiratory cycle) might therefore facilitate lymph progression in the muscular regions, accounting for the results shown in Figs 5*B* and 6*B*.

Differential recruitment of tendineous diaphragmatic lymphatics with increased serosal fluid volume

In experimental ascitis, the tracer distribution in muscular regions (data not shown) was similar to that described for the control peritoneal injection (Fig. 5*B*). Conversely, a slower and limited invasion of the tracer in the muscular regions (Fig. 8*B*), and a more homogeneous and deeper distribution within the tendinous ones (Fig. 8*C*) was found in pleural effusion. This behaviour might depend, at least partially, upon the greater stiffness of the chest wall compared to the abdominal wall. In fact, unlike the expandable abdominal walls which can accommodate large fluid volumes, the radial expansion of the thorax is limited by a rigid costal scaffold. Hence, pleural effusion tends to accumulate in the diaphragmatic apposition zones, displacing the peripheral diaphragm caudally and modifying: (a) the shape of the diaphragm; (b) the length and tension of the central tendon; and (c) the length and force exerted by muscles fibres on inspiration. It is worth recalling that not tissue displacement, but the extent of active muscle contraction seems essential for lymph formation and progression in the intercostal muscles in spontaneous ventilation (Moriondo *et al.* 2005).

Regional gravity-dependent diaphragmatic lymphatic function

While no apparent gravity-dependent differences were observed in the distribution of the tracers in control conditions and in pleural effusion, a substantially different distribution of dextrans between the ventral (region 2, Fig. 1) and dorsal (region 4, Fig. 1) tendinous regions was observed in peritoneal ascitis. In fact, while in ventral region 2 tracer invasion was only slightly modified compared to control (Fig. 7*B*), most of the dextrans being distributed in the peritoneal transverse ducts, in the dorsal region 4 the tracer localized mostly in the pleural transverse ducts. The faster invasion of the dorsal tendineous lymphatics when P_{abd} is increased in supine rats, might reflect a greater recruitment of lymphatics in the tendinous regions due to an increased cavity-to-lymphatic driving pressure gradient.

Summary

In conclusion, the present data suggest that, although the whole diaphragmatic lymphatic system is directly involved in the process of fluid and solute removal from the pleural and peritoneal serous cavities, preferential recruitment of regional lymphatics occurs in relation to the functional draining requirements. Although the highest stomata and lacunae density is localized in the central tendinous compartment of the diaphragm, the removal of pleural and peritoneal fluid and solutes in normal steady state seems to be mainly accounted for by the muscular diaphragmatic lymphatics. Conversely, in pleural or peritoneal effusions, an increased fluid and solute drainage is achieved not only through a passive increase of the driving pressure gradients, but also though a more consistent recruitment of the tendinous lymphatics, probably ensuring a greater-volume capacity. This recruitment strategy suggests that the diaphragmatic lymphatic system is specifically designed to efficiently exploit the local changes in tissue stress as an extrinsic mechanism to support lymph formation and propulsion under both normal and pathophysiological circumstances.

References

Aukland K & Reed R (1993). Interstitial-lymphatic mechanisms in the control of extracellular fluid volume. *Physiol Rev* **73**, 1–78.

Bridenbaugh EA, Gashev AA & Zawieja DC (2003). Lymphatic muscle: a review of contractile function. *Lymphat Res Biol* **1**, 147–158.

Gashev AA, Davis MJ, Delp MD & Zawieja DC (2004). Regional variations of contractile activity in isolated rat lymphatics. *Microcirculation* **11**, 477–492.

Grimaldi A, Moriondo A, Sciacca L, Guidali ML, Tettamanti G & Negrini D (2006). Functional arrangement of rat diaphragmatic initial lymphatic network. *Am J Physiol Heart Circ Physiol* **291**, H876–H885.

Lai-Fook SJ, Houtz PK & Jones PD (2005). Transdiaphragmatic transport of tracer albumin from peritoneal to pleural liquid measured in rats. *J Appl Physiol* **99**, 2212–2221.

Mariassy A & Wheeldon E (1983). The pleura: a combined light microscopy, scanning and transmission electron microscopy study in sheep. *I. Normal pleura. Exp Lung Res* **4**, 293–314.

Michailova K (2001). Postinflammatory changes of the diaphagmatic stomata. *Ann Anat* **183**, 309–317.

Miserocchi G, Mariani E & Negrini D (1982). Role of the diaphragm in setting liquid pressure in serous cavities. *Respir Physiol* **50**, 381–392.

Miserocchi G, Negrini D & Mortola J (1984). Comparative features of Starling–lymphatic interaction at the pleural level in mammals. *J Appl Physiol* **56**, 1151–1156.

Miserocchi G, Negrini D, Mukenge S, Turconi P & Del Fabbro M (1989). Liquid drainage through the peritoneal diaphragmatic surface. *J Appl Physiol* **66**, 1579–1585.

Moriondo A, Mukenge S & Negrini D (2005). Transmural pressure in rat initial subpleural lymphatics during spontaneous or mechanical ventilation. *Am J Physiol Heart Circ Physiol* **289**, H263–H269.

Negrini D, Ballard ST & Benoit JN (1994). Contribution of lymphatic myogenic activity and respiratory movements to pleural lymph flow. *J Appl Physiol* **76**, 2267–2274.

Negrini D & Del Fabbro M (1999). Subatmospheric pressure in the rabbit pleural lymphatic network. *J Physiol* **520**, 761–769.

Negrini D, Del Fabbro M, Gonano C, Mukenge S & Miserocchi G (1992). Distribution of diaphragmatic lymphatic lacunae. *J Appl Physiol* **72**, 1166–1172.

Negrini D, Del Fabbro FM & Venturoli D (1993). Fluid exchanges across the parietal peritoneal and pleural mesothelia. *J Appl Physiol* **74**, 1779–1784.

Negrini D, Moriondo A & Mukenge S (2004). Transmural pressure during cardiogenic pressure oscillations in rodent diaphragmatic lymphatic vessels. *Lymph Res Biol* 2.

Negrini D, Mukenge S, Del Fabbro M, Gonano C & Miserocchi G (1991). Distribution of diaphragmatic lymphatic stomata. *J Appl Physiol* **70**, 1544–1549.

Ohtani Y, Ohtani O & Nakatani T (1993). Microanatomy of the rat diaphragm: a scanning and confocal laser scanning microscopic study. *Arch Histol Cytol* **56**, 317–328.

Schmid-Schöenbein G (1990). Microlymphatics and lymph flow. *Physiol Rev* **70**, 987–1019.

Wang NS (1975). The preformed stomata connecting the pleural cavity and the lymphatics in the parietal pleura. *Am Rev Respiratory Dis* **111**, 12–20.

Wang N (1998). Anatomy of the pleura. *Clin Chest Med* **19**, 229–240.

von der Weid PY & Zawieja DC (2004). Lymphatic smooth muscle: the motor unit of lymph drainage. *Int J Biochem Cell Biol* **36**, 1147–1153.

Zawieja DC, Davis KI, Schuster R, Hinds WM & Granger HJ (1993). Distribution, propagation and coordination of contractile activity in lymphatics. *Am J Physiol Heart Circ Physiol* **264**, H1283–H1291.

Acknowledgements

This research was funded by the Italian Ministry of the University and of Scientific and Technological Research (MIUR, contract FAR 2003; FIRB 2001, contract RBAU01L4MZ). Dr Laura Sciacca work was funded by a contract from MIUR (FIRB 2001, contract RBAU01L4MZ).